Emergence and percolation of rigid domains during the colloidal glass transition

Xiunan Yang,[1,2,*] Hua Tong,[3,*] Wei-Hua Wang,[4,2,5,†] and Ke Chen[1,2,5,‡]

[1]*Beijing National Laboratory for Condensed Matter Physics and Key Laboratory of Soft Matter Physics, Institute of Physics, Chinese Academy of Sciences, Beijing 100190, People's Republic of China*

[2]*University of Chinese Academy of Sciences, Beijing 100049, People's Republic of China*

[3]*Department of Fundamental Engineering, Institute of Industrial Science, University of Tokyo, 4-6-1 Komaba, Meguro-ku, Tokyo 153-8505, Japan*

[4]*Institute of Physics, Chinese Academy of Sciences, Beijing 100190, People's Republic of China*

[5]*Songshan Lake Materials Laboratory, Dongguan, Guangdong 523808, China*

(Received 29 January 2018; revised manuscript received 27 June 2018; published 28 June 2019)

Using video microscopy, we measure local spatial constraints in disordered binary colloidal samples, ranging from dilute fluids to jammed glasses, and probe their spatial and temporal correlations to local dynamics during the glass transition. We observe the emergence of significant correlations between constraints and local dynamics within the Lindemann criterion, which coincides with the onset of glassy dynamics in supercooled liquids. Rigid domains in fluids are identified based on local constraints and demonstrate a percolation transition near the glass transition, accompanied by the emergence of dynamical heterogeneities. Our results show that spatial constraint instead of the geometry of amorphous structures is the key that connects the complex spatial-temporal correlations in disordered materials.

DOI: 10.1103/PhysRevE.99.062610

A liquid solidifies when sufficiently cooled. Under near-equilibrium conditions, crystals form, with distinctively different structures and mechanical properties than those of the liquid phase. When rapidly quenched, on the other hand, a supercooled liquid undergoes glass transition and becomes an amorphous solid with apparently disordered structures. For the glass transitions, two fundamental questions remain. The first one is "when does a supercooled liquid qualitatively transform into a solid during the glass transition?'. Glasses obviously fit our experiences with solids. Experimentally, however, there is no definitive point of solidification, despite more than 10 orders of magnitude increase in viscosity during the glass transition. The other question is "what structural orders, if any, are associated with the unusual dynamical phenomena and the rise of rigidity during the glass transition?" Many studies attempt to construct structural parameters based on local geometry to distinguish slow rigid domains from more mobile fluid regions in glasses [1–5], but have yet to find any universal signatures.

In condensed matters, particularly in solids, the role of the structure is to confine the motion of atoms, thus to maintain rigidity. From this point of view, a solid loses its rigidity when the motions of consisting atoms can no longer be adequately constrained. A perfect example is the Lindemann criterion for the melting of crystals, which is found to be accurate in almost all crystalline materials [6,7]. A crystal melts when the vibrational fluctuations of atoms reach the order of one tenth of the lattice constant. The Lindemann criterion is independent of the symmetry of the underlying structures of the solids, thus may be employed to determine the liquid-solid transition in glass-forming materials [8–20]. In metastable structures, the vibrational fluctuations of atoms are primarily determined by local structures, thus the confinement experienced by individual particles can be employed as a structural parameter when the geometry is too intricate to analyze.

In this paper, we employ the local Debye-Waller factor to measure the local constraints in colloidal liquids and glasses, and investigate its correlations to local dynamics during the glass transition. Temporal correlations between particle constraints and local dynamics reveal the emergence of structural relaxation barriers that give rise to finite rigidity in the system as the temperature decreases. A common Lindemann-like length scale is identified by measuring the configurational changes when the system overcomes the relaxation barriers and starts behaving like fluids. The rise of rigidity and the onset of glassy dynamics are both shown to coincide with the percolation of rigid domains identified by the Lindemann-like length scale. Dynamical heterogeneity increases sharply when rigid domains percolate the system, and then decreases when the system becomes overwhelmingly solid. Our results suggest that a Lindemann-like criterion can be applied in amorphous materials to determine the transition between liquid and solid states, and the glass transition is the growth and percolation of rigid domains in supercooled liquids.

The samples consist of binary mixtures of poly-N-isopropylacrylamide (PNIPAM) particles [21,22] hermetically sealed between two cover slips, forming a monolayer of disordered packing. To avoid crystallization, the diameter ratio between large and small particles is chosen to be 1:1.4, with the number ratio close to 1. The PNIPAM particles are thermosensitive which allows the *in situ* tuning of the packing

*These authors contributed equally to this work.
†whw@iphy.ac.cn
‡kechen@iphy.ac.cn

fractions using an objective heater (BiOptechs). PNIPAM spheres are best described as hard spheres with soft shells [21,23]. At high packing fractions, PNIPAM particles are compressible to some extent, allowing observation of dynamical phenomena above the hard sphere jamming transition. The diameters of the particles are measured by dynamical light scattering to be 1 and 1.4 μm at 22 °C. The total number of particles in the field of view is about 3500. To cover a wide range of packing fractions, two groups of samples are separately prepared. The packing fractions are between 0.890 and 0.850 (jammed solids) for the first group, and between 0.56 and 0.84 (unjammed liquids) for the second group. Here we use the two-dimensional jamming packing fraction of hard spheres of 0.85 to indicate that no spontaneous topological rearrangements are observed in samples of higher packing fractions during the time window available to our experiments [24]. Before data acquisition, the samples are equilibrated on a microscope stage for 3 h. The particle configurations are recorded by digital video microscopy on a Leica DMI 6000B microscope with an oil objective with numerical aperture (NA) of 1.40, at frame rates of 30–110 frames/s. The digital resolution of the acquired images is 0.1 μm/pixel, and the particle trajectories are extracted by particle-tracking techniques [25]. Combined optical and tracking error of particle fluctuations is estimated to be less than 0.01 μm by measuring the mean-square displacement (MSD) of fixed particles at different packing fractions.

Spatial constraints felt by individual particles can be measured by either the lowest energy barrier for displacements or positional fluctuations. For jammed samples, the phonon modes are extracted using the covariance matrix analysis [26–28]. Briefly, we define a time-averaged covariance matrix $C_{ij} = \langle |\delta \mathbf{r_i}(t)\rangle \langle \delta \mathbf{r_j}(t)| \rangle_t$, where $\delta \mathbf{r_i}(t)$ is the particle displacement from its equilibrium position, and $i, j = 1, \ldots, 2N$ run over all particles and x (y) coordinates. The covariance matrix C_{ij} is directly related to the dynamical matrix D_{ij} under the harmonic approximation, with $D_{ij} = \frac{k_B T \langle C^{-1}\rangle_{ij}}{\sqrt{m_i m_j}}$, where m_i is the mass of particle i. Diagonalization of the dynamical matrix yields the phonon frequencies and eigenvectors of a "shadow system" of the same configurations and interactions as the colloids in experiment, but without the damping. In jammed solids with stable configurations, the lowest energy barrier is directly related to the soft phonon modes [29]. We employ a soft-mode parameter Ψ for individual particles, proposed by Tong and Xu [30,31] based on the equipartition hypothesis. For particle i, $\Psi_i^{2N} = \sum_{j=1}^{2N} \frac{1}{\omega_j^2} |\vec{e}_{j,i}|^2$, where ω_j is the vibrational frequency of mode j and $\vec{e}_{j,i}$ is the polarization vector of particle i in mode j, and N is the number of particles in a two-dimensional glass. Positional fluctuations are characterized by the Debye-Waller factor $\alpha_i(\tau) = \langle [\vec{r}_i(\tau + t_0) - \vec{r}_i(t_0)]^2 \rangle$, where $\vec{r}_i(t_0)$ is the position of particle i at time t_0, and $\langle . \rangle$ denotes the average for trajectories starting with different t_0 [30,32]. The Debye-Waller factor is often employed as a dynamical parameter. On short timescales when topological rearrangement is infrequent, the local Debye-Waller factor is primarily determined by local structures, thus it can be employed as a structural parameter as well. Previous experiments and simulations have shown that short-time local positional fluctuation is a good predictor of long-time dynamics in the supercooled and glass regime [32,33].

In the following, we show that Ψ_i^{2N} is statistically proportional to the single-particle Debye-Waller factor α_i in metastable glasses. At low temperatures, the system can be considered fluctuating around the reference state $|\mathbf{r}_0\rangle$ which sits in a local minimum of the potential energy landscape. We denote the j_{th} eigenvector as $|\vec{e}_j\rangle$ with the eigenfrequency ω_j. The equation of motion is

$$|\delta \ddot{\mathbf{r}}(t)\rangle + D|\delta \mathbf{r}(t)\rangle = 0. \tag{1}$$

Here $|\delta \mathbf{r}(t)\rangle = |\mathbf{r}(t)\rangle - |\mathbf{r}_0\rangle$ is the displacement from the reference state. The solution of Eq. (1) can be written as a superposition of the normal modes

$$|\delta \mathbf{r}(t)\rangle = \sum_j A_j e^{-i\sqrt{D}t} |\vec{e}_j\rangle = \sum_j A_j e^{-i\omega_j t} |\vec{e}_j\rangle, \tag{2}$$

where $A_j = \langle \vec{e}_j | \delta \mathbf{r}(0)\rangle$ is the amplitude of the projection of initial displacement on mode j. The important condition required by thermodynamics at equilibrium is that the energy is equally distributed among all the modes. Therefore, we have for each mode the kinetic energy $mA_j^2\omega_j^2/2 = k_B T/2$, which leads to $A_j^2 = k_B T/m\omega_j^2$. The local Debye-Waller factor is calculated

$$\begin{aligned} \alpha_i(\tau) &= \langle [\vec{r}_i(\tau + t_0) - \vec{r}_i(t_0)]^2 \rangle \\ &= \langle [\delta \vec{r}_i(\tau + t_0) - \delta \vec{r}_i(t_0)]^2 \rangle \\ &= \langle \delta \vec{r}_i(\tau + t_0)^2 \rangle - 2\langle \delta \vec{r}_i(\tau + t_0) \cdot \delta \vec{r}_i(t_0) \rangle \\ &\quad + \langle \delta \vec{r}_i(t_0)^2 \rangle. \end{aligned} \tag{3}$$

Since the normal modes are excited by thermal noise, we substitute Eq. (2) into Eq. (3) and apply the random phase approximation. The second term in Eq. (3) vanishes, which leads to

$$\alpha_i = 2\sum_j A_j^2 \vec{e}_{j_i} \cdot \vec{e}_{j,i} = \frac{2k_B T}{m_i} \sum_j \frac{1}{\omega_j^2} |\vec{e}_{j,i}|^2. \tag{4}$$

Except for the overall proportional coefficient, the right side of Eq. (4) is just the soft-mode parameter Ψ_i.

The high correlations between soft mode Ψ and Debye-Waller factor α are experimentally demonstrated in jammed colloidal glasses. Figure 1(a) plots Spearman's rank correlation between Ψ_i^n and α_i as a function of the fraction of the lowest frequency modes $\frac{n}{2N}$ included in jammed colloidal glasses. The correlation to local dynamics comes predominantly from the lowest frequency modes, as the bottom 0.5% of modes (~30 for our system) achieve a correlation over 0.8. The inset of Figure 1(a) plots the correlation between Ψ_i^{30} and α_i at different packing fractions, which shows that in jammed solids, positional fluctuations of individual particles can be well described by a handful of soft modes. Figure 1(b) shows the spatial distribution of cooperatively rearranging regions (CRRs) composed of the top 10% fastest particles (white circles) [34] and Ψ_i^{30} (colored contours). It is clear that regions with higher concentrations of soft modes are spatially correlated with fast local dynamics.

In jammed glasses, soft modes can be accounted for by short-time fluctuations of particle positions. Figure 1(c) plots

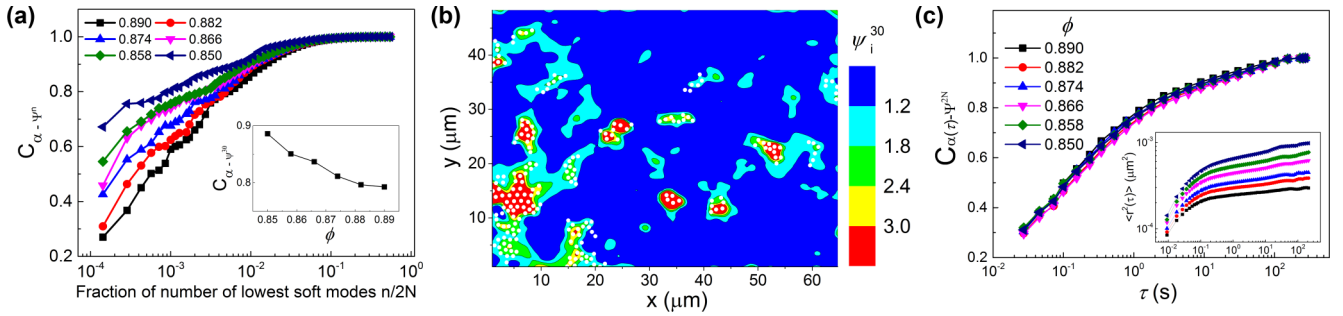

FIG. 1. Correlation between soft mode and Debye-Waller factor in jammed packings. (a) Correlation between α_i and Ψ_i^n as a function of the fraction of the lowest frequency modes $n/2N$ included in Ψ_i^n at different packing fractions. Inset: correlations between α and Ψ^{30} at different packing fractions. The noise level is about 0.02. (b) Real space distribution of cooperatively rearranging regions (white dots) and Ψ^{30} at $\phi = 0.850$ (colored contours), normalized by the average value. (c) Rank correlations between Ψ_i^{2N} and $\alpha_i(\tau)$ as a function of τ for different packing fractions. The noise level is about 0.02. Inset: MSDs at different ϕ.

the correlation between $\alpha_i(\tau)$ and Ψ_i^{2N} as a function of the time window τ in which α_i is measured. The correlation increases rapidly for small τ values and reaches ∼0.8 at ∼1s, within the β-relaxation timescale (∼10s) defined by the middle of the plateau in the log-log plot of the mean-square displacements [Fig. 1(c), inset] [32]. During this small time window, the positional fluctuations of the particles are significantly greater than the optical, tracking, and drifting errors in the experiments. The high correlations between short-time $\alpha_i(\tau)$ and Ψ_i^{2N} suggest that the local structures can be adequately explored at relatively short periods of time. Thus short-time particle Debye-Waller factor can be employed as an effective soft-mode parameter in colloidal systems below jamming [35], where direct measurements of spatial distribution of soft modes are difficult.

We now apply $\alpha_i(\tau)$ in unjammed colloidal liquids to measure local mechanical constraints. As particles are diffusive with changing local environments in unjammed fluids, there are significant variations of the fluctuations of the same particle over time. For liquids, we employ $\alpha_i(\tau, t_0) = [\vec{r}_i(\tau + t_0) - \vec{r}_i(t_0)]^2$; $\alpha_i(\tau, t_0)$ is no longer averaged over t_0, and is a function of both t_0 and τ. To identify the relevant timescales over which local structures have the most influence over future dynamics in liquids, we measure the temporal correlations between $\alpha_i(t_0, \tau)$ and local dynamics measured by nonaffine displacement $D^2_{\min}(\Delta t)$ [36,37] after the preceding structures are measured. $D^2(t_1, t_2) = \sum_n \sum_i [r^i_{n,t_2} - r^i_{0,t_2} - \sum_j (\delta_{ij} + \varepsilon_{ij}) \times (r^j_{n,t_1} - r^j_{0,t_1})]^2$, where $r^i_{n,t}$ is the ith (x or y) component of the position of the nth particle at time t, and the $\delta_{ij} + \varepsilon_{ij}$ that minimize D^2 are calculated based on $r^i_{n,t}$. $D^2_{\min}$ measures the particle level nonaffine strain, i.e., the minimum mean square difference between actual relative displacements of particle to its neighbors and the relative displacements that they would have if they were in a region of uniform strain. The correlation between $\alpha_i(t_0, \tau)$ and $D^2_{\min}$ is averaged over trajectories starting from different t_0.

Correlations between $\alpha_i(t_0, \tau)$ and $D^2_{\min}(\Delta t)$ depend on both the window τ in which structural information is collected, and Δt, the timescale of the dynamics after α_i is measured. Figure 2 plots the correlations between α_i and $D^2_{\min}$ averaged from trajectories starting from different t_0 as a function of τ and Δt in liquids of different packing fractions. The highest correlations are achieved at $\tau_{\max}$, indicated by grey dashed lines. $\tau_{\max}$ is thus the proper timescale to identify structures that have the highest predictability for dynamics in liquids. For observation window shorter than $\tau_{\max}$, insufficient structural information is collected, and for much longer time windows, relevant information will eventually be lost in structural relaxations. In our experiments, $\tau_{\max}$ is found to be in the vicinity of β-relaxation time τ_β, indicated by white dashed lines. The β-relaxation time and α-relaxation time of the samples are extracted by fitting the intermediate scattering function $F_s(q, t) = \langle \sum_{i=1}^N e^{i\widehat{\mathbf{q_m}} \cdot [x_i(t) - x_i(0)]} \rangle_\theta / N$ with a two-step stretched exponential function (the Kohlrausch-Williams-Watts function) [38,39]. Here $x_j(t)$ is the position of particle i at time t, N is the number of particles, $\mathbf{q_m}$ is the scattering vector determined by the first peak in the structural factor, and $\langle . \rangle_\theta$ indicates an average over 120 evenly distributed directions of $\mathbf{q_m}$. For liquids with only one-step relaxations, the fitting of the function yields two nearly identical relaxation times.

Figure 3(a) plots the correlation between $\alpha_i(t_0, \tau_{\max})$ and $D^2_{\min}(\Delta t)$ as a function of Δt. At low packing fractions, the correlation between α_i and local dynamics is low, and it decays almost immediately after the α_i is measured. This short memory in dynamics reflects a nearly flat potential energy landscape where structural relaxations are facilitated by free diffusion and collisions between particles. The energy landscape becomes more rugged as the packing fraction increases, and an activation mechanism begins to emerge [40]. At higher packing fractions, the correlation between α_i and $D^2_{\min}$ first increases with Δt then decreases after reaching a peak value at Δt_{act}. This delayed correlation peak between local constraints and structural relaxations signifies the emergence of rearranging barriers, hence finite rigidity of the system, with Δt_{act} being the average time required for thermal fluctuations to overcome the barriers for structural relaxations. When the packing fraction is further increased, the energy barrier also increases, with higher peak correlation values. Figure 3(a) is obtained using the tracking algorithm developed by Crocker and Grier [25]. We also applied three other published tracking algorithms by van der Wel and Kraft, Lu *et al.*, and Gao and Kilfoil respectively [41–43], and obtained nearly identical correlation curves from the microscopy data.

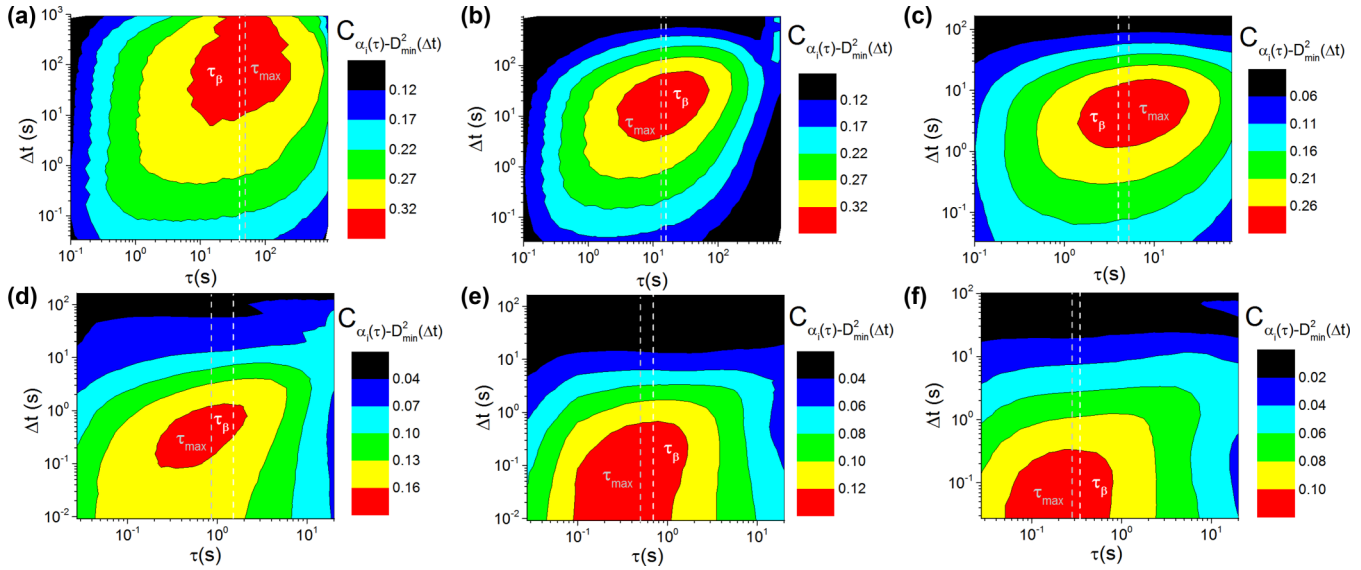

FIG. 2. Structure-dynamics correlation $C_{\alpha_i(t_0,\tau)-D^2_{\min}(\Delta t)}$ averaged from trajectories starting from different t_0 as a function of Δt and τ in liquids. The packing fractions are (a) 0.84, (b) 0.79, (c) 0.74, (d) 0.69, (e) 0.63, and (f) 0.56. The white dashed line indicates the β-relaxation time τ_β and the grey dashed line indicates the $\tau_{\max}$ for each packing fraction.

The rise of the relaxation barriers coincides with the separation of α- and β-relaxation timescales in liquids [44]. Figure 3(b) plots the measured τ_α, τ_β, and $\Delta t_{\rm act}$ in unjammed colloidal samples. The increase of the relaxation time is modest near the jamming point compared to standard hard-sphere systems [45,46], due to the softness of PNIPAM spheres. Below $\phi = 0.69$, $\Delta t_{\rm act}$ is short, and the τ_α and τ_β are close. Without obvious peaks, $\Delta t_{\rm act}$ is chosen to be the point where the correlation between α_i and $D^2_{\rm min}$ starts to decay, as indicated by vertical arrows in Fig. 3(a). Between the packing fraction of 0.63 and 0.69, the α- and β-relaxation times begin to separate, indicating the onset of glassy dynamics; and a pronounced correlation peak appears for $\phi = 0.69$. $\Delta t_{\rm act}$ becomes significantly larger than τ_β when the packing fraction is further increased. As the α_i is measured on the timescale of $\tau_{\max}$ (close to τ_β), a $\Delta t_{\rm act}$ greater than τ_β allows the prediction of long-time dynamics with short-time structural information.

Temporally, local dynamics in liquids begin to decouple from earlier structures after $\Delta t_{\rm act}$. An interesting question is whether the average positional fluctuations of the particles reach a common length scale when the system begins to behave like a fluid, as in the case of the melting of crystals. In Figure 3(c), we replot the $C_{\alpha_i - D^2_{\rm min}}$ as a function of system MSDs. For all the packing fractions, the correlation begins to decay around 17% of the averaged particle diameter d indicated by the dashed line, close to the Lindemann criterion for the melting of crystals [6], despite orders of magnitude differences in relaxation timescales between these liquid samples. We can thus define $L = 0.17d$ as the equivalent melting criterion for glasses, and generalize the Lindemann criterion from the melting of crystals to the transition between solid and fluid phases in amorphous materials [7–20] where the dichotomy between solid and fluid phases has been ambiguous. For a given time window, structures that evolve less than the

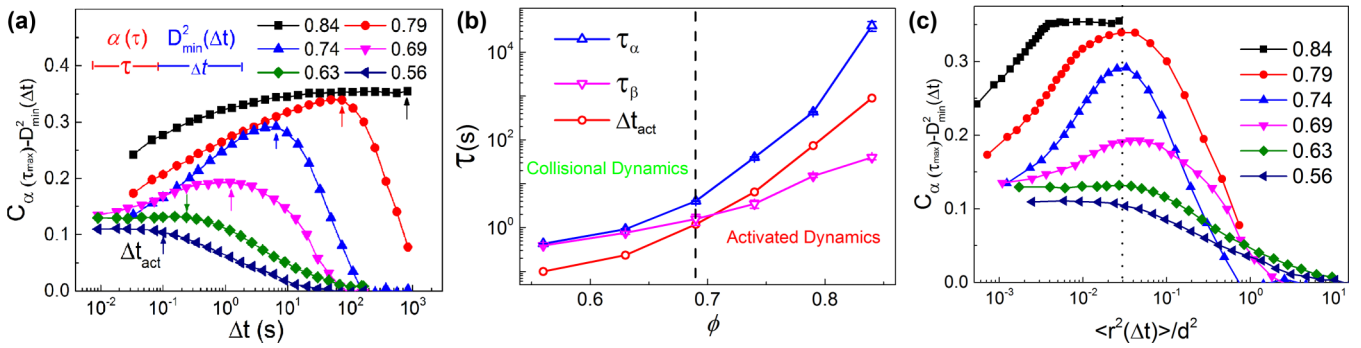

FIG. 3. Structure-dynamics correlation during the glass transition. (a) Spearman's rank correlation between $\alpha_i(t_0, \tau_{\max})$ and $D^2_{\rm min}(\Delta t)$ as a function of Δt. The correlations are averaged from trajectories starting from different t_0. The vertical arrows indicate the $\Delta t_{\rm act}$ when the correlations start to decay. Inset: the time sequence for measuring $\alpha(t_0, \tau)$ and $D^2_{\rm min}(\Delta t)$. (b) ϕ dependence of the activation time $\Delta t_{\rm act}$, and the α and β relaxation time. The dashed line indicates the onset of glassy dynamics. (c) Structure-dynamic correlation $C_{\alpha_i(t_0,\tau_{\max})-D^2_{\rm min}(\Delta t)}$ as a function of MSDs normalized by the corresponding mean diameter at each packing fraction. Vertical dotted line indicates the Lindemann criterion. The noise level is about 0.02.

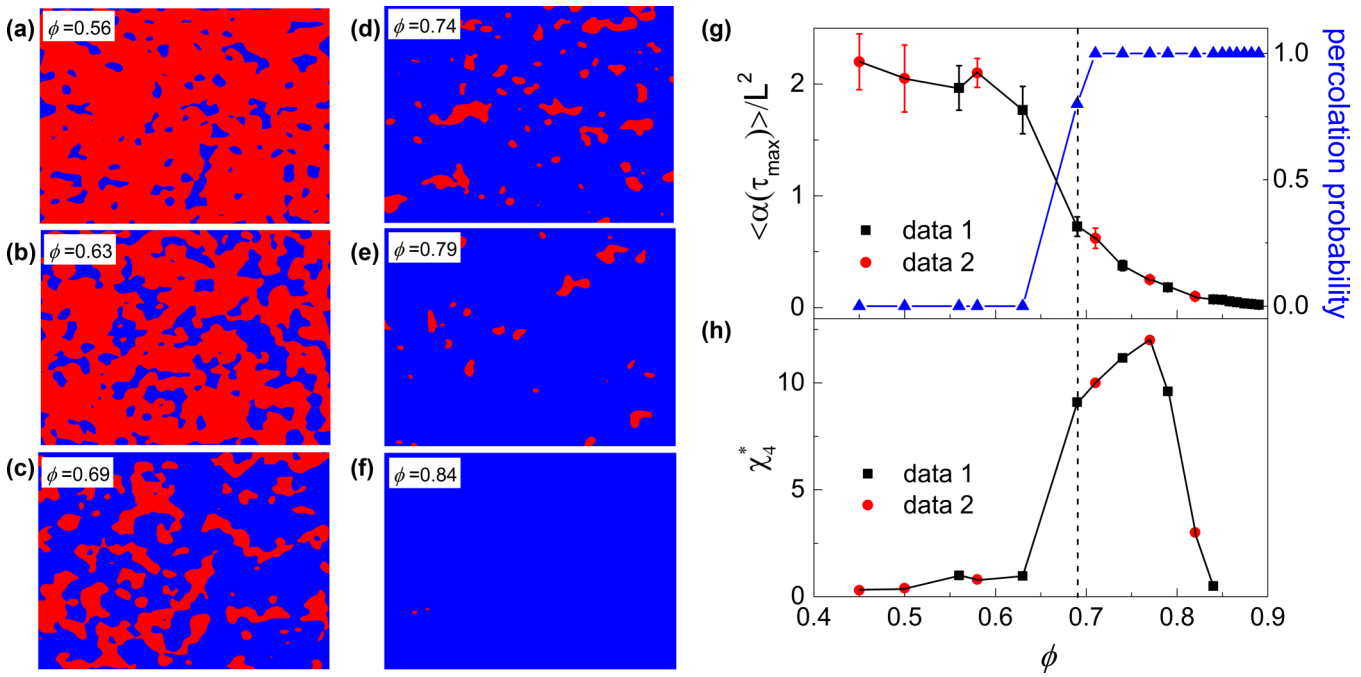

FIG. 4. Structure evolution during the glass transition. (a)–(f) Spatial distribution of $\alpha_i(t_0, \tau_{\max})$ at different packing fractions, binarized by the Lindemann criterion. Red colors are fluid regions with $\alpha_i(t_0, \tau_{\max})$ larger than the Lindemann criterion; blue colors are rigid regions with $\alpha_i(t_0, \tau_{\max})$ below the Lindemann criterion. (g) Average $\alpha_i(t_0, \tau_{\max})$ and the percolation of rigid regions during glass transition. Left axis: average $\alpha_i(t_0, \tau_{\max})$ normalized by Lindemann criterion, as a function of ϕ. The dashed line indicates the onset of glassy dynamics shown in Fig. 3(b). The black squares (data 1) are measured from the same dataset as in Figs. 1 and 2. To extend the range of the plot, we include measurements from an additional dataset (data 2, red circles). Error bars represent standard deviations. Right axis: the probability of rigid regions percolating the field of view (blue triangles). The probability is calculated as the fraction of the configurations with rigid regions percolating the field of view in all measured configurations. (h) Peak value of dynamical susceptibility χ_4^* as a function of ϕ.

L are considered solid-like or rigid, while structures evolving more than the L are considered fluid-like.

Before applying the Lindemann-like criterion locally to identify rigid or fluidic domains, a proper observation time window needs to be determined. In the original Lindemann theory for crystals, the vibrational fluctuations of atoms around equilibrium positions are considered. For glasses, atoms can be considered primarily vibrating in cages on the β-relaxation timescale. However, instead of arbitrarily imposing the β-relaxation time, we employ $\tau_{\max}$, which naturally emerges as the timescale most pertinent to future dynamics from intercorrelation measurement, as the observation window for the identification of rigid regions. As shown in Fig. 2, $\tau_{\max}$ at different packing fractions are very close to the measured β-relaxation times.

Using the time window of $\tau_{\max}$, we identify solid-like domains in unjammed samples whose $\alpha_i(t_0, \tau_{\max})$ are below the Lindemann criterion, and fluid regions with higher $\alpha_i(t_0, \tau_{\max})$ during the glass transition. Figures 4(a)–4(f) plot the snapshots of the spatial distribution of $\alpha_i(t_0, \tau_{\max})$ at different packing fractions, binarized by the Lindemann criterion. Bond percolation based on the particle positions is used after we cluster rigid particles from the nearest neighbors which are determined from the first minimum of the radial distribution function. At low packing fractions, the system is mostly fluid-like (red color) with small pockets of solid-like regions (blue color). The rigid regions grow with the packing fraction and begin to percolate the system around $\phi = 0.69$ until complete solidification near the jamming point.

Key features of the percolation phase transition are recovered by analyzing the distributions of the size and shape of the solid-like clusters, which suggests that the glass transition can be described by classical percolation phase transitions. Figure 5(a) plots the distribution of cluster size of the rigid domains before percolation. The distributions can be well fitted by a power-law function with an exponential cutoff. The power-law exponent is 0.7, independent of packing fraction. The probability to observe large clusters is higher than randomly generated clusters, as plotted in Fig. 5(b), which suggests that particles in rigid domains are spatially correlated. Figure 5(c) plots the cluster size and radius of gyration of rigid clusters, which show a universal fractal dimension of 1.78 for all packing fractions before percolation. Both the maximum and mean cluster sizes diverge when approaching a critical packing fraction $\phi_c = 0.69$, as plotted in Fig. 5(d), the fitted power-law exponnt is -3.58 for both characteristic sizes. Thus, the evolution of rigid domains in two-dimensional colloidal glasses shows the hallmarks of a continuous phase transition, with striking similarities to the observations in solid-liquid transition of three-dimensional colloidal crystals [47]. The percolation probability of rigid regions and the averaged $\alpha_i(t_0, \tau_{\max})$ of the system shows a sharp transition around $\phi = 0.69$, as plotted in Fig. 4(g).

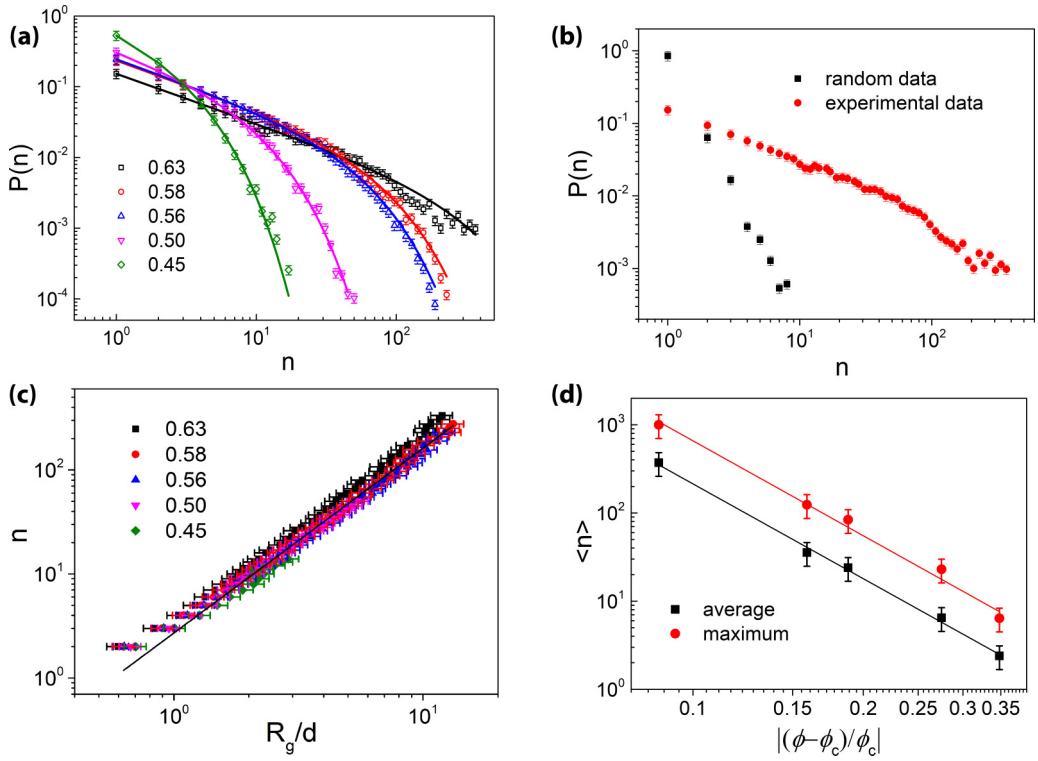

FIG. 5. Distribution of the size and shape of rigid clusters approaching the percolation. (a) Cluster size distributions $P(n)$ of rigid clusters before percolation; drawn lines are fits to a power-law distribution with exponential cutoff. (b) Comparison of experimental $P(n)$ for $\phi = 0.63$ (red circles) and a distribution for a randomly generated distribution with the same number of rigid particles (black squares). (c) Cluster size n as a function of radius of gyration R_g normalized by average particle diameter d at ϕ from 0.45 to 0.63; drawn line indicates a fractal dimension of 1.78. (d) Characteristic cluster size $\langle n \rangle$ taken as the time-averaged size of the largest cluster (circles) or the time- and ensemble-averaged size of all clusters (square) as a function of packing fraction; lines indicates a power-law fit to $\langle n \rangle \propto |(\phi - \phi_c)/\phi_c|^{-3.58}$.

The growth and percolation of the rigid regions in cooling liquids provide a microscopic origin for the onset of glassy dynamics shown in Fig. 3(a) and the dynamical heterogeneity. At low packing fractions, isolated rigid structures are created and relaxed by a one-step fluctuation-relaxation process. The size and the fraction of rigid regions both increase as the samples are further cooled. At a critical packing fraction ($\phi = 0.69$ in our experiments), the rigid regions become connected and percolate the system [48,49]. Before the percolation, isolated rigid domains exist in the liquid. However, unconnected rigid clusters cannot render the whole system rigid, as they are simply floating in a continuous phase of flowing liquid. Only after the percolation, the ability of the spanning network of rigid domains to resist small stresses gives rise to finite rigidity of the whole system. For the relaxation dynamics, before percolation, the rigid domains are formed and relaxed locally through fluctuations in the liquid, with a single relaxation time. After the percolation, while the liquid relaxation process remains in the liquid phase, the relaxation of the system-wide rigid network is much harder than that of isolated rigid clusters, which results in a much longer relaxation time, namely, the α-relaxation time. The percolating rigid network also impedes long-distance diffusions of particles. Under spatial confinement, particles are forced to rearrange locally through cooperative motions, or β relaxation [34,50,51]. The decoupling of relaxation times signals the transition from a local relaxation process to a correlated relaxation process [52,53]. Dynamical heterogeneity naturally emerges from the competition between these two different relaxation mechanisms [54]. The peak of the dynamical susceptibility χ_4^* first increases around $\phi = 0.69$ and then decreases near the jamming point ($\phi_j \sim 0.85$) when the whole system becomes homogeneously rigid [55], as plotted in Fig. 4(h) [56,57]).

In summary, by measuring the local constraints in colloidal liquids and glasses, we directly observe the emergence and growth of structure-dynamics correlations in supercooled liquids, which depend on a Lindemann-like length scale in configurational changes. The glass transition is then shown to be the growth and percolation of the rigid regions in supercooled liquids, which can be employed to explain the slowing down and the dynamical heterogeneity [54,58]. Although our results are obtained from a quasi-two-dimensional hard-sphere colloidal system, the method to identify solid-like regions in fluids can be easily generalized to other glassy systems. Following the melting analogy, the rigid clusters in the glass transition are similar to crystalline nuclei during crystallization. These clusters are also natural candidates for low-entropy droplets in random first-order transition theories for their slower dynamics [9]. We thus speculate the percolation of rigid domains during the glass transition can also be observed in three-dimensional glasses [46,59–62] or in systems with different interactions, while the specific path

leading to the percolation or the evolution of the connected rigid network after it may be different, which will be an interesting topic for future simulation or experimental studies. Our results are strong evidence that local constraints are a useful parameter to connect structure to dynamics in glassy systems compared to purely geometric or topological metrics. A direct link between conventional geometric structures and glassy dynamics may be established by searching for local and nonlocal configurations that contribute the most to local constraints in glassy materials [63].

We thank Walter Kob, Peter Harrowell, Rui Liu, Mingcheng Yang, Chenhong Wang, and Maozhi Li for helpful discussions. We thank Yongxiang Gao and Mathieu Leocmach for helping with the tracking algorithms. This work was supported by the MOST 973 Program (No. 2015CB856800). K.C. also acknowledges support from the NSFC (No. 11474327, No. 11874395). H.T. acknowledges the support from the Japan Society for the Promotion of Science (JSPS) Postdoctoral Fellowship.

[1] F. Spaepen, A microscopic mechanism for steady state inhomogeneous flow in metallic glasses, Acta Metall. **25**, 407 (1977).
[2] H. Tanaka, T. Kawasaki, H. Shintani, and K. Watanabe, Critical-like behaviour of glass-forming liquids, Nat. Mater. **9**, 324 (2010).
[3] H. W. Sheng, W. K. Luo, F. M. Alamgir, J. M. Bai, and E. Ma, Atomic packing and short-to-medium-range order in metallic glasses, Nature **439**, 419 (2006).
[4] K. F. Kelton, G. W. Lee, A. K. Gangopadhyay, R. W. Hyers, T. J. Rathz, J. R. Rogers, M. B. Robinson, and D. S. Robinson, First X-Ray Scattering Studies on Electrostatically Levitated Metallic Liquids: Demonstrated Influence of Local Icosahedral Order on the Nucleation Barrier, Phys. Rev. Lett. **90**, 195504 (2003).
[5] Y.-C. Hu, F.-X. Li, M.-Z. Li, H.-Y. Bai, and W.-H. Wang, Five-fold symmetry as indicator of dynamic arrest in metallic glass-forming liquids, Nat. Commun. **6**, 8310 (2015).
[6] F. A. Lindemann, The calculation of molecular eigenfrequencies, Phys. Z. **11**, 609 (1910).
[7] S. Alexander, Amorphous solids: Their structure, lattice dynamics and elasticity, Phys. Rep. **296**, 65 (1998).
[8] H. B. Yu, R. Richert, R. Maa, and K. Samwer, Unified Criterion for Temperature-Induced and Strain-Driven Glass Transitions in Metallic Glass, Phys. Rev. Lett. **115**, 135701 (2015).
[9] X. Xia and P. G. Wolynes, Fragilities of liquids predicted from the random first order transition theory of glasses, Proc. Natl. Acad. Sci. USA **97**, 2990 (2000).
[10] C. Angell, Formation of Glasses from Liquids and Biopolymers, Science **267**, 1924 (1995).
[11] W. Gotze, Recent tests of the mode-coupling theory for glassy dynamics, J. Phys.: Condens. Matter **11**, A1 (1999).
[12] R. Hall and P. Wolynes, The aperiodic crystal picture and free energy barriers in glasses, J. Chem. Phys. **86**, 2943 (1987).
[13] F. H. Stillinger, A topographic view of supercooled liquids and glass formation, Science **267**, 1935 (1995).
[14] R. Berry and B. Smirnov, Phase transitions and adjacent phenomena in simple atomic systems, Phys. Usp. **48**, 345 (2005).
[15] F. Starr, S. Sastry, J. F. Douglas, and S. C. Glotzer, What do we Learn from the Local Geometry of Glass-Forming Liquids? Phys. Rev. Lett. **89**, 125501 (2002).
[16] V. Novikov and A. Sokolove, Universality of the dynamic crossover in glass-forming liquids: A "magic" relaxation time, Phys. Rev. E **67**, 031507 (2003).
[17] V. N. Novikov, E. Rössler, V. K. Malinovsky, and N. V. Surovtsev, Strong and fragile liquids in percolation approach to the glass transition, Europhys. Lett. **35**, 289 (1996).
[18] J. Dyre, Colloquium: The glass transition and elastic models of glass-forming liquids, Rev. Mod. Phys. **78**, 953 (2006).
[19] J. Onuchic, Z. Luthey-Schulten, and P. Wolynes, Theory of protein folding: The energy landscape perspective, Annu. Rev. Phys. Chem. **48**, 545 (1997).
[20] L. Larini Ottochian, C. De Michelle, and D. Leporinin, Universal scaling between structural relaxation and vibrational dynamics in glass-forming liquids and polymers, Nat. Phys. **4**, 42 (2008).
[21] P. J. Yunker, K. Chen, M. D. Gratale, M. A. Lohr, T. Still, and A. G. Yodh, Physics in ordered and disordered colloidal matter composed of poly(N-isopropyl acrylamide) microgel particles, Rep. Prog. Phys. **77**, 056601 (2014).
[22] K. Chen, T. Still, S. Schoenholz, K. B. Aptowicz, M. Schindler, A. C. Maggs, A. J. Liu, and A. G. Yodh, Phonons in two-dimensional soft colloidal crystals, Phys. Rev. E **88**, 022315 (2013).
[23] Y. Han, N. Y. Ha, A. M. Alsayed, and A. G. Yodh, Melting of two-dimensional tunable-diameter colloidal crystals, Phys. Rev. E **77**, 041406 (2008).
[24] Z. Zhang, N. Xu, D. T. N. Chen, P. Yunker, A. M. Alsayed, K. B. Aptowicz, P. Habdas, A. J. Liu, S. R. Nagel, and A. G. Yodh, Thermal vestige of the zero-temperature jamming transition, Nature **459**, 230 (2009).
[25] J. C. Crocker and D. G. Grier, Methods of digital video microscopy for colloidal studies, J. Colloid Interface Sci. **179**, 298 (1996).
[26] S. Henkes, C. Brito, and O. Dauchot, Extracting vibrational modes from fluctuations: A pedagogical discussion, Soft Matter **8**, 6092 (2012).
[27] K. Chen *et al.*, Low-Frequency Vibrations of Soft Colloidal Glasses, Phys. Rev. Lett. **105**, 025501 (2010).
[28] K. Chen, M. L. Manning, P. J. Yunker, W. G. Ellenbroek, Z. Zhang, A. J. Liu, and A. G. Yodh, Measurement of Correlations between Low-Frequency Vibrational Modes and Particle Rearrangements in Quasi-Two-Dimensional Colloidal Glasses, Phys. Rev. Lett. **107**, 108301 (2011).
[29] N. Xu, V. Vitelli, A. J. Liu, and S. R. Nagel, Anharmonic and quasi-localized vibrations in jammed solids - Modes for mechanical failure, Europhys. Lett. **90**, 56001 (2010).
[30] H. Tong and N. Xu, Order parameter for structural heterogeneity in disordered solids, Phys. Rev. E **90**, 010401(R) (2014).
[31] H. Tong, H. Hu, P. Tan, N. Xu, and H. Tanaka, Revealing Inherent Structural Characteristics of Jammed Particulate Packings, Phys. Rev. Lett. **122**, 215502 (2019).

[32] A. Widmer-Cooper and P. Harrowell, Predicting the Long-Time Dynamic Heterogeneity in a Supercooled Liquid on the Basis of Short-Time Heterogeneities, Phys. Rev. Lett. **96**, 185701 (2006).
[33] R. Pastore, G. Pesce, A. Sasso, and M. Pica Ciamarra, Cage size and jump precursors in glass-forming liquids: Experiment and simulations, J. Phys. Chem. Lett. **8**, 1562 (2017).
[34] G. Adam and J. H. Gibbs, On the temperature dependence of cooperative relaxation properties in glass-forming liquids, J. Chem. Phys. **43**, 139 (1965).
[35] R. L. Jack, A. J. Dunleavy, and C. P. Royall, Information-Theoretic Measurements of Coupling between Structure and Dynamics in Glass Formers, Phys. Rev. Lett. **113**, 095703 (2014).
[36] X. Yang, R. Liu, M. Yang, W.-H. Wang, and K. Chen, Structures of Local Rearrangements in Soft Colloidal Glasses, Phys. Rev. Lett. **116**, 238003 (2016).
[37] M. L. Falk and J. S. Langer, Dynamics of viscoplastic deformation in amorphous solids, Phys. Rev. E **57**, 7192 (1998).
[38] J. Mattsson, H. M. Wyss, A. Fernandez-Nieves, K. Miyazaki, Z. B. Hu, D. R. Reichman, and D. A. Weitz, Soft colloids make strong glasses, Nature **462**, 83 (2009).
[39] T. Kawasaki and H. Tanaka, Structural evolution in the aging process of supercooled colloidal liquids, Phys. Rev. E **89**, 062315 (2014).
[40] V. Lubchenko, Theory of the structural glass transition: A pedagogical review, Adv. Phys. **64**, 283 (2015).
[41] C. van der Wel and D. J. Kraft, Automated tracking of colloidal clusters with sub-pixel accuracy and precision, J. Phys.: Condens. Matter **29**, 044001 (2017).
[42] P. J. Lu, M. Shutman, E. Sloutskin, and A. V. Butenko, Locating particles accurately in microscope images requires image-processing kernels to be rotationally symmetric, Opt. Express **21**, 30755 (2013).
[43] Y. Gao and M. L. Kilfoil, Accurate detection and complete tracking of large populations of features in three dimensions, Opt. Express **17**, 4685 (2009).
[44] P. G. Debenedetti and F. H. Stillinger, Supercooled liquids and the glass transition, Nature **410**, 259 (2001).
[45] R. Pastore, G. Pesce, and M. Caggioni, Differential variance analysis: A direct method to quantify and visualize dynamic heterogeneities, Sci. Rep. **7**, 43496 (2017).
[46] S. Vivek, C. P. Kelleher, P. M. Chaikin, and E. R. Weeks, Long-wavelength fluctuations and the glass transition in two dimensions and three dimensions, Proc. Natl. Acad. Sci. USA **114**, 1850 (2017).
[47] J. Sprakel, A. Zaccone, F. Spaepen, P. Schall, and D. A. Weitz, Direct Observation of Entropic Stabilization of bcc Crystals Near Melting, Phys. Rev. Lett. **118**, 088003 (2017).
[48] M. H. Cohen and G. S. Grest, Liquid-glass transition, a free-volume approach, Phys. Rev. B **20**, 1077 (1979).
[49] D. J. Jacobs and M. F. Thorpe, Generic Rigidity Percolation: The Pebble Game, Phys. Rev. Lett. **75**, 4051 (1995).
[50] S. Albert *et al.*, Fifth-order susceptibility unveils growth of thermodynamic amorphous order in glass-formers, Science **352**, 1308 (2016).
[51] C. Crauste-Thibierge, C. Brun, F. Ladieu, D. L'Hôote, G. Biroli, and J.-P. Bouchaud, Evidence of Growing Spatial Correlations at the Glass Transition from Nonlinear Response Experiments, Phys. Rev. Lett. **104**, 165703 (2010).
[52] R. Pastore, A. Coniglio, A. de Candia, A. Fierro, and M. Pica Ciamarra, Cage-jump motion reveals universal dynamics and non-universal structural features in glass forming liquids, J. Stat. Mech. (2016) 054050.
[53] R. Pastore, G. Pesce, A. Sasso, and M. P. Ciamarra, Many facets of intermittent dynamics in colloidal and molecular glasses, Colloids Surf. A **532**, 87 (2017).
[54] D. Long, and F. Lequeux, Heterogeneous dynamics at the glass transition in van der Waals liquids, in the bulk and in thin films, Eur. Phys. J. E **4**, 371 (2001).
[55] P. Ballesta, A. Duri, and L. Cipelletti, Unexpected drop of dynamical heterogeneities in colloidal suspensions approaching the jamming transition, Nat. Phys. **4**, 550 (2008).
[56] R. Candelier, O. Dauchot, and G. Biroli, Building Blocks of Dynamical Heterogeneities in Dense Granular Media, Phys. Rev. Lett. **102**, 088001 (2009).
[57] Z. Zhang, P. J. Yunker, P. Habdas, and A. G. Yodh, Cooperative Rearrangement Regions and Dynamical Heterogeneities in Colloidal Glasses with Attractive Versus Repulsive Interactions, Phys. Rev. Lett. **107**, 208303 (2011).
[58] G. Biroli, J.-P. Bouchaud, K. Miyazaki, and D. R. Reichman, Inhomogeneous Mode-Coupling Theory and Growing Dynamic Length in Supercooled Liquids, Phys. Rev. Lett. **97**, 195701 (2006).
[59] P. Harrowell, Nonlinear physics: Glass transitions in plane view, Nat. Phys. **2**, 157 (2006).
[60] B. Illing, S. Fritschi, H. Kaiser, C. L. Klix, G. Maret, and P. Keim, Mermin-Wagner fluctuations in 2D amorphous solids, Proc. Natl. Acad. Sci. USA **114**, 1856 (2017).
[61] H. Shiba, Y. Yamada, T. Kawasaki, and K. Kim, Unveiling Dimensionality Dependence of Glassy Dynamics: 2D Infinite Fluctuation Eclipses Inherent Structural Relaxation, Phys. Rev. Lett. **117**, 245701 (2016).
[62] H. Tong and H. Tanaka, Revealing Hidden Structural Order Controlling Both Fast and Slow Glassy Dynamics in Supercooled Liquids, Phys. Rev. X **8**, 011041 (2018).
[63] S. S. Schoenholz, E. D. Cubuk, D. M. Sussman, E. Kaxiras, and A. J. Liu, A structural approach to relaxation in glassy liquids, Nat. Phys. **12**, 469 (2016).